ENGINEERING

Acousto-dielectric tweezers enable independent manipulation of multiple particles

Liang Shen[1,2], Zhenhua Tian[2]*, Kaichun Yang[1], Joseph Rich[3], Jinxin Zhang[1], Jianping Xia[1], Wesley Collyer[1], Brandon Lu[1], Nanjing Hao[1], Zhichao Pei[1], Chuyi Chen[1], Tony Jun Huang[1]*

Acoustic tweezers have gained substantial interest in biology, engineering, and materials science for their label-free, precise, contactless, and programmable manipulation of small objects. However, acoustic tweezers cannot independently manipulate multiple microparticles simultaneously. This study introduces acousto-dielectric tweezers capable of independently manipulating multiple microparticles and precise control over intercellular distances and cyclical cell pairing and separation for detailed cell-cell interaction analysis. Our acousto-dielectric tweezers leverage the competition between acoustic radiation forces, generated by standing surface acoustic waves (SAWs), and dielectrophoretic (DEP) forces, induced by gradient electric fields. Modulating these fields allows for the precise positioning of individual microparticles at points where acoustic radiation and DEP forces are in equilibrium. This mechanism enables the simultaneous movement of multiple microparticles along specified paths as well as cyclical cell pairing and separation. We anticipate our acousto-dielectric tweezers to have enormous potential in colloidal assembly, cell-cell interaction studies, disease diagnostics, and tissue engineering.

INTRODUCTION

The contactless manipulation of micro/nano-objects—such as cells (*1*, *2*), droplets (*3*), synthetic multifunctional particles (*4*), and extracellular vesicles (*5*)—is a critical function desired for many disciplines, including biology (*6*, *7*), chemistry (*8*), pharmacy (*9*), and engineering (*10*, *11*). So far, various techniques have been developed to achieve contactless micro/nano-object manipulation, such as optical (*12*–*14*), optoelectronic (*15*, *16*), electric (*17*–*19*), magnetic (*20*, *21*), and acoustic tweezers (*2*, *22*–*26*). Among these contactless tweezing techniques, acoustic tweezers have recently gained significant interest from researchers due to its label-free nature, high biocompatibility, low power consumption, and high feasibility of manipulating various objects with different material properties (*27*–*31*). In particular, surface acoustic wave (SAW) tweezers offer additional advantages such as easy integration with lab-on-a-chip devices (*32*, *33*), enhanced spatial resolution enabled by higher operating frequencies (*34*), and customizable transducer designs for added versatility (*35*). With these features, various SAW tweezing devices have been developed for a wide range of applications, such as three-dimensional translation (*2*), patterning (*36*–*40*), separation (*41*–*45*), sorting (*46*–*49*), and rotation of micro/nano-objects (*50*–*52*).

Despite considerable advancements in the field of acoustic tweezers, most tweezing mechanisms synchronously manipulate multiple particles trapped in acoustic potential wells (*2*, *53*). For example, when using the most common phase modulation-based particle translation mechanism, multiple particles trapped in a grid-like array of Gor'kov potential wells are synchronously moved following the same translation pattern. Similarly, chirped acoustic tweezers, which leverage the frequency modulation-based particle translation mechanism, also synchronously move multiple particles trapped in an array of potential wells (*22*). To achieve independent manipulation of multiple single particles, the phased array concept (*54*, *55*) has recently been introduced for acoustic tweezers development. Although there has been success in achieving independent manipulation of multiple single objects in the air using airborne acoustic waves generated from low-frequency transducer arrays, there are currently no phased arrays that can independently manipulate multiple single microparticles or cells with microscale translation resolution in liquids. On the other hand, acoustic holography-based mechanisms (*34*, *56*, *57*) have been introduced to develop acoustic tweezing devices for selectively trapping and translating a microparticle among multiple microparticles in a microfluidic chamber. However, these holography-based devices are not able to independently manipulate multiple microparticles.

To overcome the aforementioned limitations, this study presents unique acousto-dielectric tweezers that enable simultaneous and independent manipulation of multiple micrometer-sized particles or cells within a microfluidic chamber. In particular, our acousto-dielectric tweezers leverage two pairs of interdigital transducers (IDTs) arranged orthogonally to generate and control standing SAWs with grid-like energy distributions (*2*) and multiple groups of four-port electrodes with each group to generate and tune a local electric field in an area surrounded by the four-port electrodes (*58*). Therefore, microparticles or cells are subjected to both acoustic radiation and dielectrophoretic (DEP) forces. Their equilibrium positions depend on the competition between acoustic radiation and DEP forces, and the change of these positions can be achieved by controlling the competition. Compared to existing acoustic tweezers, our acousto-dielectric tweezers introduce local electric fields and enable simultaneous and independent manipulation of multiple single micro-objects.

To understand the mechanism of our acousto-dielectric tweezers for single microparticle manipulation, both numerical simulations were performed to analyze the combined acoustic radiation (*59*, *60*) and DEP forces (*61*) applied on a microparticle, and experiments were conducted to investigate the particle translation under different force combinations. Our results show that the equilibrium position (i.e., trapping position) of a microparticle subjected to both

[1]Department of Mechanical Engineering and Materials Science, Duke University, Durham, NC 27708, USA. [2]Department of Mechanical Engineering, Virginia Polytechnical Institute and State University, Blacksburg, VA 24061, USA. [3]Department of Biomedical Engineering, Duke University, Durham, NC 27708, USA.
*Corresponding author. Email: tianz@vt.edu (Z.T.); tony.huang@duke.edu (T.J.H.)

acoustic radiation and DEP forces can be precisely shifted in the *x*-*y* plane by adjusting the input voltages for the four-port electrodes surrounding the particle manipulation region without changing the standing SAW field.

To demonstrate the ability to independently manipulate multiple single microparticles or cells, we manufactured a device having two orthogonal pairs of IDTs to generate standing SAWs and four groups of four-port electrodes with each group surrounding a Gor'kov potential well (*2*) to generate and tune the local electric field overlapping with the potential well. By independently tuning the local electric fields in four Gor'kov potential wells, microparticles preloaded into those wells were simultaneously and independently translated along different pre-defined paths. Moreover, by reducing the SAW wavelength, the electric field modulation region surrounded by a group of four-port electrodes can overlap with multiple Gor'kov potential wells, thus enabling more complex manipulation functions. For example, when the electric field modulation region contained two Gor'kov potential wells, we experimentally demonstrated precise control over the intercellular distance between two trapped cells, allowing for the cyclical pairing and separation of these two cells.

RESULT

Mechanism of acousto-dielectric tweezers

The acousto-dielectric tweezers utilize the competition between acoustic radiation and DEP forces applied on micrometer-sized particles or cells to transport them controllably. Figure 1A gives a schematic of an acousto-dielectric tweezing chip composed of two pairs of IDTs orthogonally positioned along the *x* and *y* axes and a set of four-port electrodes deposited on a lithium niobate ($LiNbO_3$) substrate (*62*) and a polydimethylsiloxane (PDMS)–based microfluidic chamber. Using this chip, a microparticle or cell loaded in the region of interest, i.e., the area surrounded by four-port electrodes, can be controllably and precisely translated in *x* and *y* directions.

The IDTs are for generating standing SAWs with a grid lattice–like distribution of Gor'kov potential wells that can trap microparticles using acoustic radiation forces, as depicted in Fig. 1A. By carefully adjusting the excitation phases for the IDTs, the position of a Gor'kov potential well can be shifted (*53*), so that it overlaps with the region surrounded by the four-port electrodes, and its center is close to a corner of that region. The four electrodes are for controlling the electric field in the region surrounded by these electrodes. When one of the four electrodes, E_1^1, E_2^1, E_3^1, or E_4^1 (the superscript indicates device number, and the subscript indicates electrode number going clockwise), is applied with an alternating current (ac) signal and the other three electrodes are grounded, a nonuniform electric field is generated to apply a negative DEP force on a neutrally charged microparticle or cell, thus transporting in the $+x$, $-y$, $-x$, or $+y$ direction toward the position with the lowest electric field magnitude.

Therefore, when both the SAW and local electric fields are generated, a particle can be trapped at an equilibrium position, which is between the Gor'kov potential well's center and the position with the lowest electric field magnitude, as well as depends on the competition between acoustic radiation and DEP forces. Therefore, by

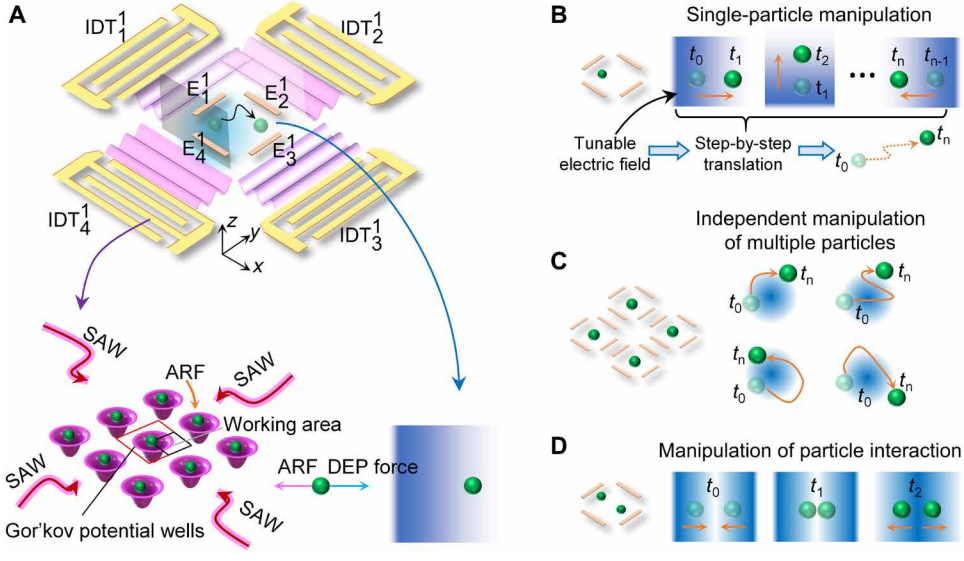

Fig. 1. Schematic illustrating the mechanism of acousto-dielectric tweezers. (**A**) Schematic of an acousto-dielectric tweezing device composed of two orthogonal pairs of IDTs including {IDT$_1^1$, IDT$_3^1$} and {IDT$_2^1$, IDT$_4^1$}, as well as a set of electrodes {E$_1^1$, E$_2^1$, E$_3^1$, E$_4^1$}. When the two pairs of IDTs are activated, standing SAWs are generated to create Gor'kov potential wells to trap particles using acoustic radiation forces. Applying AC signals to E$_1^1$ and E$_2^1$ and grounding E$_3^1$ and E$_4^1$ create a local gradient electric field within the region of interest, inducing a DEP force that moves particles to regions of low electric energy. Thus, when both the SAW and local electric fields are generated, particles can be moved to positions where acoustic radiation (ARF) and DEP forces are balanced. (**B**) Mechanism of translating a particle along a complex path. The region of interest, surrounded by four-port electrodes, contains a Gor'kov potential well centered near the top left corner. Precise control of particle movement is achieved by adjusting the input voltages to E$_1^1$ and E$_2^1$. For example, by increasing the voltage for E$_1^1$ (or E$_2^1$), a particle or cell subjected to both acoustic radiation and DEP forces can be translated in the $+x$ (or $-y$) direction. (**C**) Mechanism of independently transporting multiple particles. When multiple sets of the DEP electrodes are used, a particle loaded in each region of interest can be transported using the same mechanism in (B). (**D**) Mechanism of controlling the particle-particle distance. When the region of interest surrounded by a set of electrodes contains two Gor'kov potential wells, it becomes possible to control the particle-particle distance, such as pushing two particles together and separating them.

tuning the voltages or frequencies applied on the four-port electrodes, the DEP force acting on the particle can be changed, thus altering the particle's equilibrium position under both acoustic radiation and DEP forces, as illustrated in Fig. 1B. Notably, this acousto-dielectric equilibrium position exhibits exceptional stability. Perturbations generated from the acoustic streaming, viscous boundary layer, and diffusion, which significantly influence nanoscale particles, are negligible for the microscale particles and cells (*63*). Any perturbation-induced particle motion can thereby be effectively counteracted by a restoring force (acoustic radiation or DEP force). On the basis of these features, precise and robust translation of a particle following a desired arbitrary-shaped two-dimensional trajectory can be accomplished by gradually modulating the local electric field implemented by tuning the input voltages for the four-port electrodes. In addition, as the combination of the DEP effect, acoustic streaming effect (*64*), and acoustic radiation force (*59*) lead to a force component in the +z direction, the manipulated particles tend to remain in the upper portion of the microfluidic chamber.

On the basis of the acousto-dielectric tweezing mechanism, simultaneous and independent manipulation of multiple single particles can be achieved by incorporating multiple sets of four-port electrodes in the standing SAW generation domain. As illustrated in Fig. 1C, when a device is designed with multiple sets of four-port electrodes with each set overlapping with an off-center Gor'kov potential well, multiple regions of interest can be created for manipulating multiple single particles using the acousto-dielectric tweezing mechanism. Notably, as electric fields rapidly decay in most fluids, the electric field in each region of interest is predominantly influenced by its nearby electrodes, thus allowing for modulating the electric field locally in that region by changing voltages of nearby electrodes, without notable influences on the electric fields in other regions of interest. Therefore, by independently changing ac signals for different electrodes, the device with multiple regions of interest can modulate electric fields locally in those regions, for independently and concurrently manipulating multiple particles loaded in those regions as depicted in Fig. 1C.

In addition to the design where an electric field modulation region (i.e., an area surrounded by a group of four-port electrodes) overlaps with a Gor'kov potential well, the design where an electric field modulation region overlaps with multiple Gor'kov potential wells can lead to more particle manipulation capabilities. As illustrated in Fig. 1D, when the electric field modulation region contains two Gor'kov potential wells, the acousto-dielectric tweezing device enables the functions of controlling particle-particle distance, pushing two particles into contact to form a pair, and separating a pair of particles. To understand the mechanism of our acousto-dielectric tweezers, we performed finite element simulations to analyze the acoustic radiation and DEP forces applied to particles at different operation conditions. To demonstrate the unique abilities of our acousto-dielectric tweezers, a series of experiments were performed to independently translate four microparticles along different trajectories and precisely control the intercellular distance. The simulation and experimental results are presented below.

Translate a microparticle along complex paths

We numerically and experimentally explored the controllable translation of a microparticle along complex paths using acousto-dielectric tweezers. For these simulations and experiments, we used a device design (illustrated in Fig. 1A) with four IDTs denoted as IDT_1^1 to IDT_4^1 (the superscript indicates device number, and the subscript indicates IDT number going clockwise) to generate standing SAWs with a wavelength λ^1 of 300 μm and four-port electrodes to control the electric field in a region of interest (i.e., region for particle manipulation) with dimensions of $\lambda^1/4 \times \lambda^1/4$ (i.e., quarter-wave square dimensions). The excitation phases of the four IDTs are tuned, so that a pressure node is positioned at the top left corner of the $\lambda^1/4 \times \lambda^1/4$ region (see fig. S1) for effective particle manipulation within a 75 μm × 75 μm square area. Hence, when only using standing SAWs, a particle initially located at any position of the $\lambda^1/4 \times \lambda^1/4$ region should be transported to the pressure node at the top left corner. To apply a DEP force for moving a particle, the separation distance between two electrodes in a pair can extend to 20 mm (*65*). However, when designing the DEP electrodes for translating a particle using our acousto-dielectric tweezers, we should avoid designs with multiple SAW pressure nodes between the electrodes, such as those with electrode distances greater than a wavelength.

To elucidate the particle manipulation mechanism, finite element simulations were performed. As shown by the simulation result in Fig. 2A (top), when IDT_1^1 and IDT_3^1 are on, the generated *x*-axis standing SAWs have a pressure node line located at $x = 0$ μm and an antinode line at $x = \lambda^1/4 = 75$ μm. For a particle in the SAW field, the acoustic radiation force traps the particle at $x = 0$ μm, as shown in Fig. 2B (top). After introducing an electric field (Fig. 2A, bottom) by applying an ac input to the electrode E_1^1 with the remaining three electrodes grounded, the particle is subjected to a DEP force toward the $+x$ direction. Hence, under both acoustic radiation and DEP forces, the particle should be translated to a position with diminished total force, as predicted by the simulation result in Fig. 2B (bottom). Moreover, when gradually increasing the DEP force by increasing the input voltage for the electrode E_1^1, the particle's equilibrium position should be gradually shifted toward the $+x$ direction. To validate this prediction, experiments were performed. With IDT_1^1 and IDT_3^1, we gradually increased the voltage of the 1-MHz input signal for electrode E_1^1 from 5 to 10 V_{pp} (remaining electrodes grounded) and observed a 10-μm polystyrene bead initially trapped at an acoustic pressure node gradually translating toward the $+x$ direction (see Fig. 2C and movie S1). Similarly, when IDT_2^1 and IDT_4^1 were on, we showed gradual transportation of a 10-μm polystyrene bead in the $-y$ direction (see Fig. 2D and movie S1) by increasing the voltage of the 2-MHz input signal for electrode E_2^1 (remaining electrodes grounded). The particle displacements versus applied electrode voltages were analyzed with the results given in Fig. 2 (E and F). It can be seen that the particle displacements in both $+x$ and $-y$ directions exhibit linear relationships with respect to the applied input voltages. Using these linear relationships, we can quickly determine the required voltages for achieving the desired particle displacements.

Building upon the success of transporting a particle in $+x$ and $-y$ directions, we extended our study to the automated transportation of a particle along arbitrary-shaped two-dimensional paths. As shown in fig. S2, the two output channels of an arbitrary function generator were used to excite the two orthogonal pairs of IDTs, respectively. The two output channels of another arbitrary function generator were used to control the input ac signals for electrodes E_1^1 and E_2^1, respectively. The electrodes E_3^1 and E_4^1 were grounded. During the particle manipulation experiments, the voltages applied to the *x*-directional IDTs are 5 V_{pp}, while those applied to the *y*-directional IDTs are 10 V_{pp}. These inputs for IDTs were unchanged,

so that the generated SAW field was consistent, and the voltages for electrodes E_1^1 and E_2^1 were tuned for transporting a particle along desired paths. To automate the particle manipulation process, the function generators were controlled by custom MATLAB code to output signals with desired voltages, phases, and frequencies. For example, by automatically applying time-varying voltages in fig. S3 to electrodes E_1^1 and E_2^1, a 10-μm polystyrene particle can be translated from the pressure node position (top left corner) to trace a rectangular-shaped path (see Fig. 3A and movie S2). In this experiment, the action time for each moving step of the particle depends on the DEP force (*66*) and spans several seconds. While the acoustic radiation force exhibits a predictable sinusoidal distribution (*67*), the EDP force is notably influenced by the geometry of the electrodes and is difficult to predict in the whole working region. Hence, the manipulation was conducted using one-dimensional calibration (Fig. 2, C and D), resulting in a slight distortion of the rectangular path. In addition, we successfully demonstrated particle translation along more complex paths to depict letters, such as "D," "U," "K," and

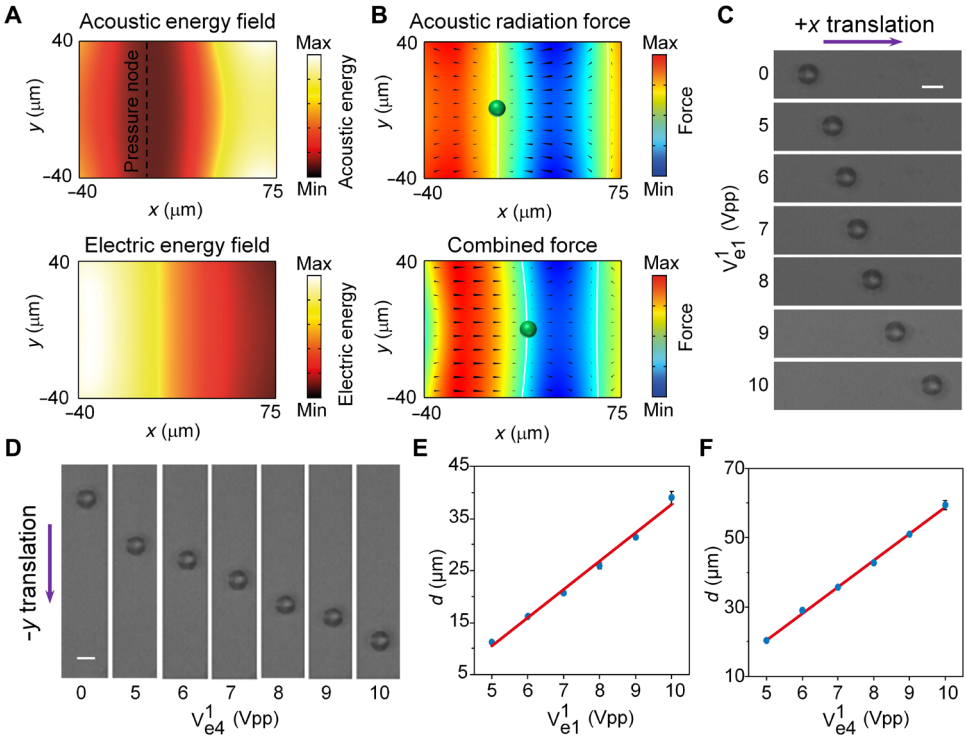

Fig. 2. Simulation and characterization results of two-dimensional transportation of a particle via acousto-dielectric tweezers. (**A**) Top: A simulated acoustic energy field of standing SAWs generated by {IDT_1^1, IDT_3^1}. This field shows a pressure node line in the low-energy region. Bottom: A simulated electric energy field, when the electrode E_1^1 is applied with an ac signal and the remaining three electrodes are grounded. The electric field gradually decays in the *x* direction and has good consistency along the *y* axis, and this field can exert an *x*-directional DEP force on a particle. (**B**) Top: A simulated acoustic radiation force field showing that a particle can be trapped on the pressure node line by the acoustic radiation force. Bottom: A simulated force field that combines acoustic radiation and DEP forces showing that a particle can be trapped at an equilibrium position with balanced acoustic radiation and DEP forces. (**C**) Time-sequential microscopic images showing a 10-μm polystyrene particle gradually translated in the +*x* direction, when increasing the input voltage on electrode E_1^1. (**D**) Time-sequential microscopic images showing the translation of a 10-μm polystyrene particle in the –*y* direction when increasing the input voltage on electrode E_2^1. During the particle translation process, input signals for all the IDTs were not changed. (**E** and **F**) Particle translation distances in +*x* and –*y* directions versus electrode input voltages, corresponding to acquired microscopic images in (C) and (D), respectively. Scale bars, 10 μm (C and D).

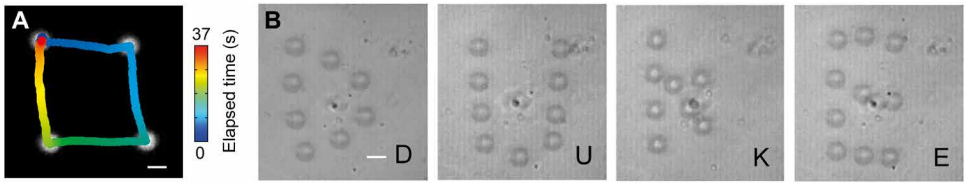

Fig. 3. Programmable transportation of a particle along complex paths via acousto-dielectric tweezers. (**A**) Result showing the automatic translation of a 10-μm fluorescent polystyrene particle to trace a square. (**B**) Stacked microscopic images showing a 10-μm polystyrene particle can be transported to depict letters D, U, K, and E. The particle translation was achieved by tuning input voltages for electrodes E_1^1 and E_2^1, and the tuning process was automatically performed by using MATLAB code to control voltage signals generated from an arbitrary function generator. Scale bars, 10 μm.

"E" (see Fig. 3B and movie S3) by using time-varying voltages given in fig. S4 (A to D, respectively). To perform these experiments, we first discretized the desired path into multiple points. Then, we determined the desired time-varying voltages for electrodes E_1^1 and E_2^1 based on the coordinates of those discrete points and the measured voltage-distance relationships in Fig. 2 (E and F). The determined time-varying voltages were applied to electrodes E_1^1 and E_2^1 for conducting the particle manipulation.

Translate multiple microparticles along different paths

In addition to manipulating a particle using a device with a set of four-port DEP electrodes, we upgraded the device design to independently and simultaneously manipulate multiple single particles to trace different arbitrary-shaped paths by incorporating multiple sets of four-port DEP electrodes. As illustrated in Fig. 4A, the upgraded acousto-dielectric tweezing device has four regions of interest (i.e., particle manipulation domains labeled with R_1 to R_4 in fig. S5) with each region surrounded by four electrodes for local electric field control. In addition, this setup is simplified by consolidating the central electrode shared by two adjacent arrays. Because two working areas share the same electrodes, as depicted in fig. S5, the distance between electrode arrays for two manipulation areas can be reduced to 0 mm. The device also has two orthogonal pairs of IDTs for generating standing SAWs. Particularly, by tuning the input phases for these IDTs, the standing SAW field is modulated, so that four pressure nodes are present in the four particle manipulation domains R_1 to R_4, respectively, and these nodes are located at the far corners from the device center, as illustrated in fig. S5.

To control the electric fields in the four regions R_1 to R_4, ac signals are applied to the outer DEP electrodes labeled with E_1^2 to E_8^2 (see Fig. 4A and fig. S5). With this approach, the input voltages for electrodes with odd subscripts can be adjusted to control the *x* positions of four different particles loaded in the four regions R_1 to R_4, respectively, and the input voltages for electrodes with even subscripts can be tuned to control the particles' *y* positions. Particularly, the electric field in each region of interest is predominantly affected by the input voltages for this region's two outer electrodes (e.g., E_1^2 and E_2^2 of the region R_1) and subjected to minimal influences from the input voltages of the remaining electrodes (e.g., E_3^2 to E_8^2). This is because our used input voltages are relatively low (e.g., 0 to 10 V_{pp}), and electric fields rapidly decay in most fluids. Consequently, our device allows for independently modulating the local electric fields in the four regions R_1 to R_4.

To better understand this independence, we performed finite element simulations. When applying the same voltage to electrodes E_1^2, E_3^2, E_5^2, and E_7^2, with the remaining electrodes grounded, the simulation result in Fig. 4B (top) shows gradient electric fields within the four regions R_1 to R_4 at the top left, top right, bottom left, and bottom right corners of the simulation domain, and the electric field intensities in the simulation domain's inner region are very low. The simulation result also shows that particles loaded in the four regions are subjected to DEP forces in predominantly $+x$, $-x$, $+x$, and $-x$ directions, respectively. On the other hand, we simulated an altered case by modifying electrode input signals for the region R_1, i.e., applying an input signal to electrode E_2^2 and grounding electrode E_1^2. Compared to the original simulation result (Fig. 4B, top), the result

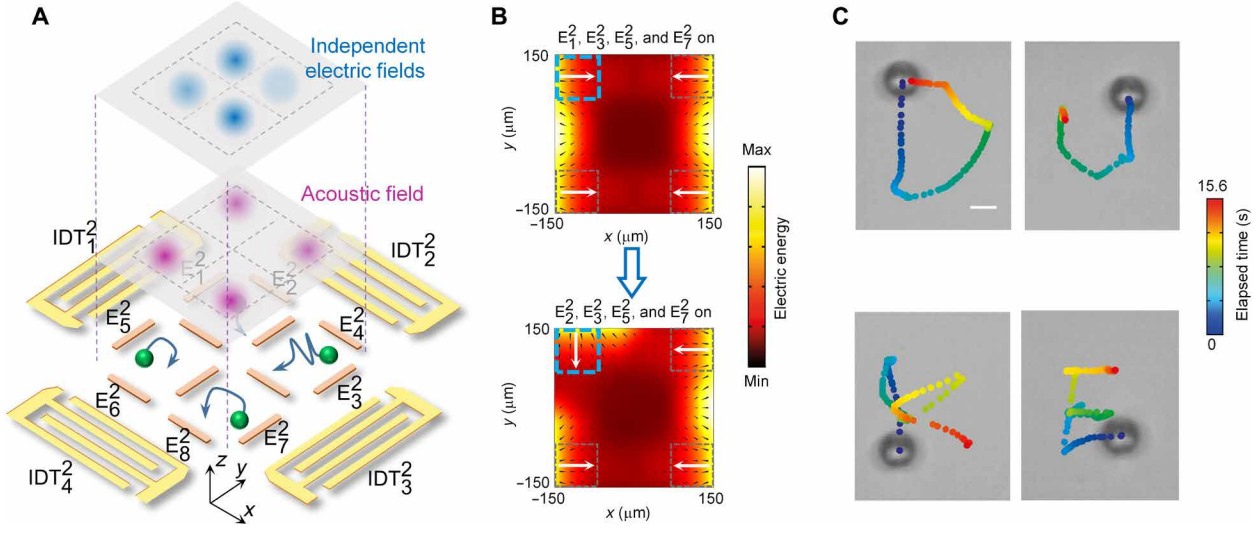

Fig. 4. Mechanism and results of using acousto-dielectric tweezers for independently manipulating multiple microparticles. (**A**) Schematic of an acousto-dielectric tweezing device with two orthogonal pairs of IDTs and an array of DEP electrodes enclosing four regions of interest. The IDTs generates standing SAWs with a Gor'kov potential well in each region. ac signals applied to outer electrodes E_1^2 to E_8^2 create local gradient electric fields, independently controlling the fields in the four regions. (**B**) Top: Simulation result showing local gradient electric fields generated in the four regions of interest (marked by dashed squares) at the simulation domain's four corners when the same ac signal is applied to electrodes E_1^2, E_3^2, E_5^2, and E_7^2, with the remaining electrodes grounded. Particles in regions R_1 to R_4 are subjected to DEP forces in $+x$, $-x$, $+x$, and $-x$ directions, respectively. Bottom: Simulated electric field when the same ac signal is applied to electrodes E_2^2, E_3^2, E_5^2, and E_7^2, with the remaining electrodes grounded. Particles in regions R_1 to R_4 are subjected to DEP forces in $-y$, $-x$, $+x$, and $-x$ directions, respectively. By comparing results in (B) top and bottom, it is evident that the local electric field in a specific region (e.g., region R_1) can be changed solely, while the electric fields in other regions (e.g., regions R_2 to R_4) remain almost unchanged. (**C**) Experiential result showing four 10-μm polystyrene particles can be transported to trace different letters D, U, K, and E simultaneously. To perform this experiment, all the IDTs were activated to generate standing SAWs, and desired input signals were applied to electrodes E_1^2 to E_8^2 automatically through four dual-channel function generators controlled by MATLAB code. Scale bar, 10 μm.

(Fig. 4B, bottom) of the altered case shows that local electric fields in regions R_2 to R_4 have negligible changes. However, the local electric field in the region R_1 is changed, and the DEP force direction changes from $+x$ to $-y$ direction. This finding indicates that the local electric fields in the four regions R_1 to R_4 can be independently modulated with negligible interference, thereby ensuring the independent manipulation of multiple particles loaded in the four regions, respectively.

For the proof of concept, we used a fabricated device (see fig. S6) to translate four 10-μm polystyrene particles in four square (75 μm by 75 μm) regions R_1 to R_4, respectively, to trace distinct paths. Particles at an approximate concentration of 1×10^6 particles/ml were introduced into the microfluidic chamber. Then, appropriate voltages were applied to the respective controlling electrodes to remove excess particles, ensuring the retention of only one particle within each manipulation region. Following this, acoustic waves were used to draw the particle into the specified acoustic potential well. Our results (Fig. 4C and movie S4) show that the four particles were successfully translated to depict letters D, U, K, and E, respectively. When conducting this experiment, 5-V_{pp} inputs were applied to the x-directional IDTs, while 10-V_{pp} inputs were applied to the y-directional IDTs. The SAW field generated by IDTs remained unchanged, and the required input signals with time-varying voltages were applied to electrodes E_1^2 to E_8^2 using multiple dual-channel function generators controlled by MATLAB code. The input signals for electrodes labeled with odd subscripts have a frequency of 1 MHz, while the input signals for electrodes with even subscripts have a frequency of 2 MHz. The required time-varying input voltages for writing the four letters are given in fig. S7 (A to D, respectively). These voltages are determined on the basis of the desired particle paths and the corresponding pre-obtained voltage-distance relationships.

Precisely control the intercellular distance

The designs described above of acousto-dielectric tweezers have a Gor'kov potential well within each region of interest surrounded by a set of four-port DEP electrodes for controllable translation of a particle within that region. When the region contains multiple Gor'kov potential wells, acousto-dielectric tweezers are able to offer more particle manipulation functions such as controlling the intercellular distance, as well as pairing and separating two cells. For the proof of concept, we designed a device (see Fig. 5A) that could generate two Gor'kov potential wells with a distance of 48 μm within a region surrounded by four-port DEP electrodes. The manipulation region is constrained to a 48 μm^2 by 48 μm^2 as illustrated in fig. S8. Numerical simulations were conducted to investigate the device-generated standing SAW field, electric field, and combined acoustic radiation and DEP force field. The simulated acoustic field (Fig. 5B, left) shows two potential wells at positions (0 μm, ±24 μm), when both x- and y-axes SAWs are generated. Note that the x-axis SAW energy is much stronger than the y-axis SAW energy, allowing for the system to center particles at $x = 0$ μm efficiently, even under the conditions with the DEP electric field turned on. Figure 5B (right) shows the simulated electric field when applying ac signals of the same voltage but different frequencies to electrodes E_2^3 and E_4^3 with electrodes E_1^3 and E_3^3 grounded. The electric energy field exhibits rapid decay from the upper and lower sides toward the middle, resulting in DEP forces whose y components can push particles toward the centerline with $y = 0$ μm. Further analysis involves investigating the combined forces exerted on particles by the acoustic and electric fields. As predicted by the simulation results in Fig. 5C, two particles originally trapped by two Gor'kov potential wells at (0 μm, ±24 μm) can be symmetrically translated to new positions on the centerline $x = 0$ μm, when applying combined acoustic radiation and DEP forces.

For validation, a pair of Jurkat cells was manipulated by our device to control their distance. When voltages of 2 V_{pp} were applied to the x-directional IDTs and 2.8 V_{pp} to the y-directional IDTs, the two cells were trapped at two pressure nodes (Fig. 5D, left). By gradually increasing the voltages of the ac signals for E_2^3 and E_4^3 from 4 to 8 V_{pp}, the intercellular distance, d_{cell}, between the cells progressively decreased until the cells were in contact, as shown by the microscope images (Fig. 5D, left to right) and internuclear distance measurements (Fig. 5E). As the cell trapping position depends on the competition between acoustic radiation and DEP forces, changing acoustic radiation forces applied on cells by changing the excitation voltage for both IDT_2^3 and IDT_4^3 can also change the intercellular distance d_{cell}. For example, by gradually increasing the voltage for IDT_2^3 and IDT_4^3 while fixing the input voltage for E_2^3 and E_4^3 at 6 V_{pp}, the intercellular distance was gradually increased due to the increased acoustic radiation forces on cells (Fig. 5F). In addition to controlling the intercellular distance, we showed the ability of our device to pair two cells (i.e., push them into contact) and separate them rapidly and cyclically, as proven by acquired microscope images (Fig. 5G) and a video of this dynamic process (movie S5). From the recorded video, the dynamic change of the intercellular distance can be evaluated (Fig. 5H), and the minimum intercellular distances at different cell-cell contact events can be analyzed (Fig. 5I).

DISCUSSION

Previous technologies using acoustic waves alone were not able to independently transport multiple microscale objects tracing different paths. To address this limitation, we have developed acousto-dielectric tweezers, which leverage the competition between acoustic radiation and DEP forces induced by acoustic waves and an electric field, respectively, for achieving the ability to independently transport multiple particles along different arbitrary-shaped paths. Our acousto-dielectric tweezers also enable for the precise control of the intercellular distance, as well as the pairing and separation of two cells in a rapid, controllable, and cyclic manner. To achieve this, our acousto-dielectric tweezers leverage two orthogonal pairs of IDTs for generating standing SAWs with a grid-like distribution of Gor'kov potential wells and multiple sets of four-port electrodes with each set for controlling the local electric field in a region of interest (i.e., domain for particle manipulation) surrounded by the four-port electrodes. When only SAWs are generated, a particle in the region of interest is subjected to an acoustic radiation force to trap it in a Gor'kov potential well. When only the local electric field is generated, the particle is subjected to a DEP force to translate it to the low electric potential region. When both the local electric field and SAWs are used, the particle can be translated to an equilibrium position that depends on the competition between counter-direction acoustic radiation and DEP forces. On the basis of this mechanism, multiple particles, which are loaded in areas surrounded by different groups of four port electrodes, respectively, can be translated independently. Moreover, the distance between two particles can be precisely controlled, and these two particles

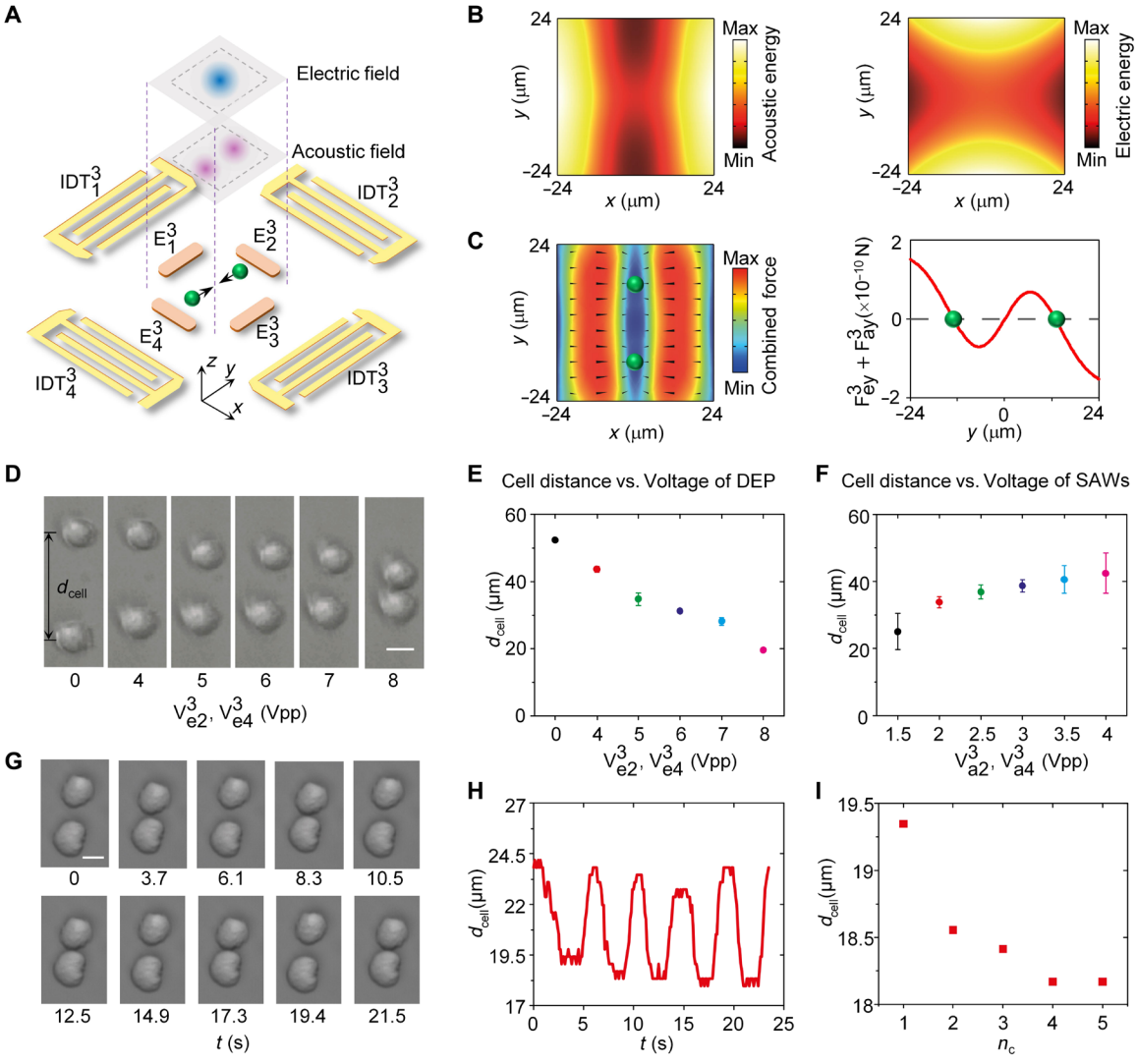

Fig. 5. Mechanism and results of using acousto-dielectric tweezers for precisely controlling the intercellular distance, as well as pairing and separating two cells. (**A**) Schematic of an acousto-dielectric tweezing device with two orthogonal pairs of IDTs and an array of DEP electrodes enclosing a region of interest for manipulating two cells. The IDTs generate standing SAWs with two Gor'kov potential wells in the region. ac signals are applied to electrodes E_1^3 and E_2^3 with E_3^3 and E_4^3 grounded, creating a gradient electric field. (**B**) Left: Simulated acoustic energy field when the *x* axis standing SAWs are stronger than the *y* axis standing SAWs. Right: Simulated electric energy field when electrodes E_2^3 and E_4^3 are applied with ac signals with the same voltage, while different frequencies and electrodes E_1^3 and E_3^3 are grounded. The electric energy decays from the upper and lower sides to the middle. (**C**) Left: Simulated force field (acoustic radiation and DEP) showing two cells positioned symmetrically on the *y* axis. Right: Distribution of combined forces along the *y* axis. (**D**) Microscope images showing the reduction of the intercellular distance between two Jurkat cells as the input voltage on electrodes E_2^3 and E_4^3 increases. (**E**) Analysis of intercellular distances in (D) versus input voltages on E_2^3 and E_4^3. (**F**) Analysis of intercellular distances versus input voltages applied on IDT$_2^3$ and IDT$_4^3$, while keeping E_2^3 and E_4^3 at 6 V_{pp}. (**G**) Microscope images showing reversible pairing and separation of two cells. (**H**) Analysis of the time-varying intercellular distance in (G). (**I**) Analysis of intercellular distances in the contact state during different pairing cycles. n_c is the index of a paring cycle. Scale bars, 10 μm (D and G).

can be pushed into contact and then separated, repeating in a cyclic manner.

Through proof-of-concept experiments, we have demonstrated the multiple functionalities of our acousto-dielectric tweezers. We successfully showed that four particles could be independently translated following different arbitrary-shaped trajectories. As the response times of both the acoustic radiation and DEP forces are less than 1 ms, changes of those forces could quickly induce corresponding cell motions. Moreover, we showed that the distance between two cells in a cell culture medium could be previously controlled. Furthermore, two target cells could be pushed into contact and then separated, and the contact/separation process could be repeated in a cyclic manner. We expect that the functions enabled by our acousto-dielectric tweezers can benefit the studies of cell-cell interaction, contact force, and communication. Given the success of in-plane particle manipulation, the out-of-plane independent manipulation of multiple particles is yet to be achieved.

The acousto-dielectric tweezing mechanism opens up a new paradigm for developing precise contactless manipulation devices. It provides an opportunity to combine the acoustic radiation and DEP

forces to address the challenges that are difficult to solve using solely one type of force. It also offers the potential for enhancing existing tweezing platforms to enable more complex manipulation of multiple particles or cells. The ac electric field and SAWs used in this study have been verified as biocompatible by numerous researchers (*17*, *33*). Beyond this work focusing on manipulating microscale particles and cells, we expect that the acousto-dielectric tweezing mechanism can be extended to the independent manipulation of multiple nanoscale objects in our future work. We also expect to improve the particle manipulation accuracy by calibrating the particle position-voltage relation and introducing a feedback control loop. In the long run, we expect this work to inspire researchers working on precision manipulation to upgrade their devices by incorporating forces stemming from different physical mechanisms. We also anticipate that the acousto-dielectric tweezers can lead to useful tools, greatly benefiting research in various fields, including colloidal assembly, cell-cell interaction, disease diagnosis, drug testing, and bioprinting.

MATERIALS AND METHODS

Device fabrication

For experimental validation, we fabricated three different sorts of acousto-dielectric tweezing chips. The first chip sort features an orthogonal pair of IDTs and a set of four-port DEP electrodes, as illustrated in Fig. 1A and fig. S1. The second chip sort features an orthogonal pair of IDTs and four regions of interest (i.e., areas for particle manipulation) surrounded by multiple DEP electrodes, as illustrated in Fig. 4A and fig. S5 (also see fig. S6 for a photo). Each IDT in these chips has 20 pairs of interdigital electrodes with a finger width of 75 μm, a finger spacing of 75 μm, and an aperture width of 3 mm. The operation frequencies of IDTs along x and y axes are 13.3 and 11.9 MHz, respectively, as the SAW speeds along these axes are different for the used Y128-cut $LiNbO_3$ piezoelectric wafer (*68*) (Y128-cut, Precision Micro-Optics). The third chip consists of a set of four-port DEP electrodes and an orthogonal pair of IDTs, as illustrated in Fig. 5A and fig. S8. Each IDT of the third chip has 20 pairs of interdigital electrodes with a finger width of 24 μm, a finger spacing of 24 μm, and an aperture width of 1 mm, and the operation frequencies of IDTs along the x and y axes are 41.7 and 37 MHz, respectively.

All the IDTs and DEP electrodes on $LiNbO_3$ substrates were fabricated with 20-nm Cr/100-nm Au layers (the Cr layer is for adhesion) following typical electron beam (e-beam) electrode fabrication procedures, which contain three main steps, i.e., photolithography, e-beam evaporation, and lift-off. In addition, each chip has a surface-bonded microfluidic chamber made of PDMS (*69*). The chamber's center coincides with the center of each IDT array on a $LiNbO_3$ substrate. All the PDMS-based microfluidic chambers with dimensions of 600 μm × 600 μm × 60 μm (length × width × height) were fabricated through typical soft lithography and mold-replica techniques.

Particle and cell sample preparation

Polystyrene particles with a diameter of 10 μm (PS010UM, MagSphere) were suspended in deionized water to an approximate concentration of 1×10^6 particles/ml. Jurkat cells (American Type Culture Collection) were maintained in RPMI-1640 medium (Gibco, Life Technologies) supplemented with 10% fetal bovine serum (Gibco, Life Technologies) and 1% penicillin-streptomycin (Mediatech). Cultures were maintained in a Heracell Vios 160i CO_2 incubator (Thermo Fisher Scientific) at 37°C with 5% CO_2. To carry out cell manipulation experiments, Jurkat cells were harvested and resuspended in a cell culture medium to an approximate concentration of 1×10^6 cells/ml.

Operation of acousto-dielectric tweezers

We conducted particle and cell manipulation experiments by using three different acousto-dielectric tweezing devices. For each experiment, the fabricated acousto-dielectric tweezing chip was mounted on the stage of an inverted optical microscope (TE2000-U, Nikon). Polystyrene particles or Jurkat cells were infused into the chamber through a 1-ml syringe (309659, Becton Dickinson). As illustrated in fig. S2, the two output channels of a dual-channel arbitrary function generator (AFG3102C, Tektronix) were directly connected to the IDTs along the x and y axes, respectively, for generating standing SAWs with the IDT resonance frequencies. For a chip with a region of interest surrounded by a set of four-port electrodes, the two channels of another dual-channel arbitrary function generator (AFG3102C, Tektronix) provided ac signals for two electrodes (i.e., E_1^1 and E_2^1 in Fig. 1A) for controlling DEP forces in x and y directions, respectively. The two other electrodes (i.e., E_3^1 and E_4^1 in Fig. 1A) are grounded. The translation of a particle or cell in a microfluidic chamber was carried out by tuning the voltages applied on the two powered electrodes. In the complex alphabet writing experiment, MATLAB code was used to control the arbitrary function generator to output ac signals with predetermined time-varying voltages automatically. For the chip with four regions of interest illustrated in Fig. 4A, we used four arbitrary function generators to simultaneously apply independent ac signals to electrode ports E_1^2 to E_8^2. During particle/cell manipulation experiments, a charge-coupled device camera (CoolSNAP) was used to acquire microscope images and record particle/cell manipulation videos.

Numerical simulation

Acousto-dielectric tweezers use both standing SAW and ac electric fields for transporting particles/cells in a microfluidic chamber. To understand the manipulation mechanism, finite element simulations were conducted using the commercial finite element software COMSOL Multiphysics. We simulated standing SAWs excited by IDTs (*64*, *70*), SAW-induced acoustic radiation forces, electric fields created by four-port electrodes, and DEP forces (*71*). The simulations of both acoustic and electric fields were carried out within a cuboid domain representing the fluid contained within a microfluidic chamber. The chamber dimensions were set to $x = 600$ μm, $y = 600$ μm, and $z = 60$ μm. To simulate the acoustic field, the COMSOL "Pressure Acoustics, Frequency Domain" module was used, and the top and side boundaries of the fluid domain were set to an impedance matching condition with an acoustic impedance of 1.04 MPa s m^{-1} (i.e., the impedance of PDMS). The bottom boundary of the fluid was set to "normal displacement" to couple the boundary displacement d_b that could be expressed as (*23*, *53*)

$$d_b = d_x \cos\left[\frac{2\pi(x - x_0)}{\lambda}\right] + d_y \cos\left[\frac{2\pi(y - y_0)}{\lambda}\right]$$

where d_x and d_y were vertical displacement of SAWs generated by IDTs along the x and y axes, respectively, and x_0 and y_0 were

locations of pressure node lines of standing SAWs along the x and y axes, respectively. To simulate the generated DEP electric field, the COMSOL "Electric Currents" module was used. Except for the electrodes, other boundaries of the simulation domain were set to "Electric Insulation" conditions for matching the electric properties of the PDMS-based microfluidic chamber wall and the substrate. "Electric Potential" conditions were used for the electrodes with input ac signals, and the remaining electrodes were grounded. The frequency-domain solver was used to solve the finite element model.

Supplementary Materials

The PDF file includes:
Figs. S1 to S10
Supplementary note
Legends for movies S1 to S5

Other Supplementary Material for this manuscript includes the following:
Movies S1 to S5

REFERENCES AND NOTES

1. D. J. Collins, C. Devendran, Z. Ma, W. Ng Jia, A. Neild, Y. Ai, Acoustic tweezers via sub–time-of-flight regime surface acoustic waves. *Sci. Adv.* **2**, e1600089 (2016).
2. F. Guo, Z. Mao, Y. Chen, Z. Xie, P. Lata James, P. Li, L. Ren, J. Liu, J. Yang, M. Dao, S. Suresh, J. Huang Tony, Three-dimensional manipulation of single cells using surface acoustic waves. *Proc. Natl. Acad. Sci. U.S.A.* **113**, 1522–1527 (2016).
3. D. J. Collins, T. Alan, K. Helmerson, A. Neild, Surface acoustic waves for on-demand production of picoliter droplets and particle encapsulation. *Lab Chip* **13**, 3225–3231 (2013).
4. J. Lipfert, S. Klijnhout, N. H. Dekker, Torsional sensing of small-molecule binding using magnetic tweezers. *Nucleic Acids Res.* **38**, 7122–7132 (2010).
5. M. Tayebi, D. Yang, D. J. Collins, Y. Ai, Deterministic sorting of submicrometer particles and extracellular vesicles using a combined electric and acoustic field. *Nano Lett.* **21**, 6835–6842 (2021).
6. Y. Zheng, J. Nguyen, Y. Wei, Y. Sun, Recent advances in microfluidic techniques for single-cell biophysical characterization. *Lab Chip* **13**, 2464–2483 (2013).
7. J. F.-C. Loo, H. P. Ho, S. K. Kong, T.-H. Wang, Y.-P. Ho, Technological advances in multiscale analysis of single cells in biomedicine. *Adv. Biosyst.* **3**, e1900138 (2019).
8. N. Hao, Z. Pei, P. Liu, H. Bachman, T. D. Naquin, P. Zhang, J. Zhang, L. Shen, S. Yang, K. Yang, S. Zhao, T. J. Huang, Acoustofluidics-assisted fluorescence-SERS bimodal biosensors. *Small* **16**, e2005179 (2020).
9. N. Hao, Z. Wang, P. Liu, R. Becker, S. Yang, K. Yang, Z. Pei, P. Zhang, J. Xia, L. Shen, L. Wang, K. A. Welsh-Bohmer, L. Sanders, L. P. Lee, T. J. Huang, Acoustofluidic multimodal diagnostic system for Alzheimer's disease. *Biosens. Bioelectron.* **196**, 113730 (2022).
10. A. Jamshidi, P. J. Pauzauskie, P. J. Schuck, A. T. Ohta, P.-Y. Chiou, J. Chou, P. Yang, M. C. Wu, Dynamic manipulation and separation of individual semiconducting and metallic nanowires. *Nat. Photonics* **2**, 86–89 (2008).
11. Y. Wu, Z. Ao, C. Bin, M. Muhsen, M. Bondesson, X. Lu, F. Guo, Acoustic assembly of cell spheroids in disposable capillaries. *Nanotechnology* **29**, 504006 (2018).
12. A. H. J. Yang, S. D. Moore, B. S. Schmidt, M. Klug, M. Lipson, D. Erickson, Optical manipulation of nanoparticles and biomolecules in sub-wavelength slot waveguides. *Nature* **457**, 71–75 (2009).
13. D. G. Grier, A revolution in optical manipulation. *Nature* **424**, 810–816 (2003).
14. J. Berthelot, S. S. Aćimović, M. L. Juan, M. P. Kreuzer, J. Renger, R. Quidant, Three-dimensional manipulation with scanning near-field optical nanotweezers. *Nat. Nanotechnol.* **9**, 295–299 (2014).
15. M. C. Wu, Optoelectronic tweezers. *Nat. Photonics* **5**, 322–324 (2011).
16. A. Puerto, A. Méndez, L. Arizmendi, A. García-Cabañes, M. Carrascosa, Optoelectronic manipulation, trapping, splitting, and merging of water droplets and aqueous biodroplets based on the bulk photovoltaic effect. *Phys. Rev. Appl.* **14**, 024046 (2020).
17. D. Kim, M. Sonker, A. Ros, Dielectrophoresis: From molecular to micrometer-scale analytes. *Anal. Chem.* **91**, 277–295 (2019).
18. H. Shafiee, J. L. Caldwell, M. B. Sano, R. V. Davalos, Contactless dielectrophoresis: A new technique for cell manipulation. *Biomed. Microdevices* **11**, 997–1006 (2009).
19. P. R. C. Gascoyne, J. Vykoukal, Particle separation by dielectrophoresis. *Electrophoresis* **23**, 1973–1983 (2002).
20. I. De Vlaminck, C. Dekker, Recent advances in magnetic tweezers. *Annu. Rev. Biophys.* **41**, 453–472 (2012).
21. J. Lipfert, X. Hao, N. H. Dekker, Quantitative modeling and optimization of magnetic tweezers. *Biophys. J.* **96**, 5040–5049 (2009).
22. S. Yang, Z. Tian, Z. Wang, J. Rufo, P. Li, J. Mai, J. Xia, H. Bachman, P.-H. Huang, M. Wu, C. Chen, L. P. Lee, T. J. Huang, Harmonic acoustics for dynamic and selective particle manipulation. *Nat. Mater.* **21**, 540–546 (2022).
23. L. Meng, F. Cai, J. Chen, L. Niu, Y. Li, J. Wu, H. Zheng, Precise and programmable manipulation of microbubbles by two-dimensional standing surface acoustic waves. *Appl. Phys. Lett.* **100**, 173701 (2012).
24. H. Junhui, A. K. Santoso, A /spl pi/-shaped ultrasonic tweezers concept for manipulation of small particles. *IEEE Trans. Ultrason. Ferroelectr. Freq. Control* **51**, 1499–1507 (2004).
25. S. Yang, J. Rufo, R. Zhong, J. Rich, Z. Wang, L. P. Lee, T. J. Huang, Acoustic tweezers for high-throughput single-cell analysis. *Nat. Protoc.* **18**, 2441–2458 (2023).
26. W. Wang, S. Li, L. Mair, S. Ahmed, T. J. Huang, T. E. Mallouk, Acoustic propulsion of nanorod motors inside living cells. *Angew. Chem. Int. Ed. Engl.* **53**, 3201–3204 (2014).
27. M. Wiklund, Acoustofluidics 12: Biocompatibility and cell viability in microfluidic acoustic resonators. *Lab Chip* **12**, 2018–2028 (2012).
28. G. Destgeer, H. J. Sung, Recent advances in microfluidic actuation and micro-object manipulation via surface acoustic waves. *Lab Chip* **15**, 2722–2738 (2015).
29. Q. Liu, J. Hu, I. V. Minin, O. V. Minin, High-performance ultrasonic tweezers for manipulation of motile and still single cells in a droplet. *Ultrasound Med. Biol.* **45**, 3018–3027 (2019).
30. P. Liu, H. Huang, X. Wang, Q. Tang, X. Qi, S. Su, Z. Xiang, J. Hu, Acoustic black hole profiles for high-performance ultrasonic tweezers. *Mech. Syst. Signal Process.* **188**, 109991 (2023).
31. J. Rufo, F. Cai, J. Friend, M. Wiklund, T. J. Huang, Acoustofluidics for biomedical applications. *Nat. Rev. Methods Primers* **2**, 30 (2022).
32. Z. Tian, Z. Wang, P. Zhang, T. D. Naquin, J. Mai, Y. Wu, S. Yang, Y. Gu, H. Bachman, Y. Liang, Z. Yu, T. J. Huang, Generating multifunctional acoustic tweezers in Petri dishes for contactless, precise manipulation of bioparticles. *Sci. Adv.* **6**, eabb0494 (2020).
33. J. Rufo, P. Zhang, R. Zhong, L. P. Lee, T. J. Huang, A sound approach to advancing healthcare systems: The future of biomedical acoustics. *Nat. Commun.* **13**, 3459 (2022).
34. M. Baudoin, J.-C. Gerbedoen, A. Riaud, B. Matar Olivier, N. Smagin, J.-L. Thomas, Folding a focalized acoustical vortex on a flat holographic transducer: Miniaturized selective acoustical tweezers. *Sci. Adv.* **5**, eaav1967 (2019).
35. P. Zhang, C. Chen, X. Su, J. Mai, Y. Gu, Z. Tian, H. Zhu, Z. Zhong, H. Fu, S. Yang, K. Chakrabarty, J. Huang Tony, Acoustic streaming vortices enable contactless, digital control of droplets. *Sci. Adv.* **6**, eaba0606 (2019).
36. A. L. Bernassau, P. G. A. MacPherson, J. Beeley, B. W. Drinkwater, D. R. S. Cumming, Patterning of microspheres and microbubbles in an acoustic tweezers. *Biomed. Microdevices* **15**, 289–297 (2013).
37. Y. Chen, X. Ding, S.-C. Steven Lin, S. Yang, P.-H. Huang, N. Nama, Y. Zhao, A. A. Nawaz, F. Guo, W. Wang, Y. Gu, T. E. Mallouk, T. J. Huang, Tunable nanowire patterning using standing surface acoustic waves. *ACS Nano* **7**, 3306–3314 (2013).
38. D. J. Collins, B. Morahan, J. Garcia-Bustos, C. Doerig, M. Plebanski, A. Neild, Two-dimensional single-cell patterning with one cell per well driven by surface acoustic waves. *Nat. Commun.* **6**, 8686 (2015).
39. D. J. Collins, R. O'Rorke, C. Devendran, Z. Ma, J. Han, A. Neild, Y. Ai, Self-aligned acoustofluidic particle focusing and patterning in microfluidic channels from channel-based acoustic waveguides. *Phys. Rev. Lett.* **120**, 074502 (2018).
40. X. Ding, J. Shi, S.-C. S. Lin, S. Yazdi, B. Kiraly, T. J. Huang, Tunable patterning of microparticles and cells using standing surface acoustic waves. *Lab Chip* **12**, 2491–2497 (2012).
41. G. Destgeer, B. H. Ha, J. H. Jung, H. J. Sung, Submicron separation of microspheres via travelling surface acoustic waves. *Lab Chip* **14**, 4665–4672 (2014).
42. X. Ding, Z. Peng, S. Lin Sz-Chin, M. Geri, S. Li, P. Li, Y. Chen, M. Dao, S. Suresh, J. Huang Tony, Cell separation using tilted-angle standing surface acoustic waves. *Proc. Natl. Acad. Sci. U.S.A.* **111**, 12992–12997 (2014).
43. S. A. Faraghat, K. F. Hoettges, M. K. Steinbach, D. R. van der Veen, W. J. Brackenbury, E. A. Henslee, F. H. Labeed, M. P. Hughes, High-throughput, low-loss, low-cost, and label-free cell separation using electrophysiology-activated cell enrichment. *Proc. Natl. Acad. Sci. U.S.A.* **114**, 4591–4596 (2017).
44. P. Li, Z. Mao, Z. Peng, L. Zhou, Y. Chen, P.-H. Huang, C. I. Truica, J. J. Drabick, W. S. El-Deiry, M. Dao, S. Suresh, T. J. Huang, Acoustic separation of circulating tumor cells. *Proc. Natl. Acad. Sci. U.S.A.* **112**, 4970–4975 (2015).
45. Y. Gu, C. Chen, Z. Mao, H. Bachman, R. Becker, J. Rufo, Z. Wang, P. Zhang, J. Mai, S. Yang, J. Zhang, S. Zhao, Y. Ouyang, D. T. W. Wong, Y. Sadovsky, T. J. Huang, Acoustofluidic centrifuge for nanoparticle enrichment and separation. *Sci. Adv.* **7**, eabc0467 (2021).
46. K. Mutafopulos, P. Spink, C. D. Lofstrom, P. J. Lu, H. Lu, J. C. Sharpe, T. Franke, D. A. Weitz, Traveling surface acoustic wave (TSAW) microfluidic fluorescence activated cell sorter (μFACS). *Lab Chip* **19**, 2435–2443 (2019).
47. D. J. Collins, A. Neild, Y. Ai, Highly focused high-frequency travelling surface acoustic waves (SAW) for rapid single-particle sorting. *Lab Chip* **16**, 471–479 (2016).

48. T. Franke, S. Braunmüller, L. Schmid, A. Wixforth, D. A. Weitz, Surface acoustic wave actuated cell sorting (SAWACS). *Lab Chip* **10**, 789–794 (2010).
49. P. Zhang, H. Bachman, A. Ozcelik, T. J. Huang, Acoustic microfluidics. *Annu. Rev. Anal. Chem.* **13**, 17–43 (2020).
50. C. Chen, Y. Gu, J. Philippe, P. Zhang, H. Bachman, J. Zhang, J. Mai, J. Rufo, J. F. Rawls, E. E. Davis, N. Katsanis, T. J. Huang, Acoustofluidic rotational tweezing enables high-speed contactless morphological phenotyping of zebrafish larvae. *Nat. Commun.* **12**, 1118 (2021).
51. D. Ahmed, A. Ozcelik, N. Bojanala, N. Nama, A. Upadhyay, Y. Chen, W. Hanna-Rose, T. J. Huang, Rotational manipulation of single cells and organisms using acoustic waves. *Nat. Commun.* **7**, 11085 (2016).
52. J. Reboud, Y. Bourquin, R. Wilson, G. S. Pall, M. Jiwaji, A. R. Pitt, A. Graham, A. P. Waters, J. M. Cooper, Shaping acoustic fields as a toolset for microfluidic manipulations in diagnostic technologies. *Proc. Natl. Acad. Sci. U.S.A.* **109**, 15162–15167 (2012).
53. Z. Tian, S. Yang, P.-H. Huang, Z. Wang, P. Zhang, Y. Gu, H. Bachman, C. Chen, M. Wu, Y. Xie, J. Huang Tony, Wave number–spiral acoustic tweezers for dynamic and reconfigurable manipulation of particles and cells. *Sci. Adv.* **5**, eaau6062 (2019).
54. R. Hirayama, D. Martinez Plasencia, N. Masuda, S. Subramanian, A volumetric display for visual, tactile and audio presentation using acoustic trapping. *Nature* **575**, 320–323 (2019).
55. A. Marzo, B. W. Drinkwater, Holographic acoustic tweezers. *Proc. Natl. Acad. Sci. U.S.A.* **116**, 84–89 (2019).
56. M. Baudoin, J.-L. Thomas, R. A. Sahely, J.-C. Gerbedoen, Z. Gong, A. Sivery, O. B. Matar, N. Smagin, P. Favreau, A. Vlandas, Spatially selective manipulation of cells with single-beam acoustical tweezers. *Nat. Commun.* **11**, 4244 (2020).
57. K. Melde, A. G. Mark, T. Qiu, P. Fischer, Holograms for acoustics. *Nature* **537**, 518–522 (2016).
58. X. Chen, Y. Ren, W. Liu, X. Feng, Y. Jia, Y. Tao, H. Jiang, A simplified microfluidic device for particle separation with two consecutive steps: Induced charge electro-osmotic prefocusing and dielectrophoretic Separation. *Anal. Chem.* **89**, 9583–9592 (2017).
59. S. Liang, W. Chaohui, H. Qiao, Force on a compressible sphere and the resonance of a bubble in standing surface acoustic waves. *Phys. Rev. E* **98**, 043108 (2018).
60. L. Zhang, From acoustic radiation pressure to three-dimensional acoustic radiation forces. *JAMA* **144**, 443–447 (2018).
61. L. Wang, L. A. Flanagan, N. L. Jeon, E. Monuki, A. P. Lee, Dielectrophoresis switching with vertical sidewall electrodes for microfluidic flow cytometry. *Lab Chip* **7**, 1114–1120 (2007).
62. Y. Q. Fu, J. K. Luo, N. T. Nguyen, A. J. Walton, A. J. Flewitt, X. T. Zu, Y. Li, G. McHale, A. Matthews, E. Iborra, H. Du, W. I. Milne, Advances in piezoelectric thin films for acoustic biosensors, acoustofluidics and lab-on-chip applications. *Prog. Mater. Sci.* **89**, 31–91 (2017).
63. M. Settnes, H. Bruus, Forces acting on a small particle in an acoustical field in a viscous fluid. *Phys. Rev. E* **85**, 016327 (2012).
64. Z. Ni, C. Yin, G. Xu, L. Xie, J. Huang, S. Liu, J. Tu, X. Guo, D. Zhang, Modelling of SAW-PDMS acoustofluidics: Physical fields and particle motions influenced by different descriptions of the PDMS domain. *Lab Chip* **19**, 2728–2740 (2019).
65. J. Kadaksham, P. Singh, N. Aubry, Manipulation of particles using dielectrophoresis. *Mech. Res. Commun.* **33**, 108–122 (2006).
66. A. Castellanos, A. Ramos, A. González, N. G. Green, H. Morgan, Electrohydrodynamics and dielectrophoresis in microsystems: Scaling laws. *J. Phys. D* **36**, 2584–2597 (2003).
67. H. Bruus, Acoustofluidics 7: The acoustic radiation force on small particles. *Lab Chip* **12**, 1014–1021 (2012).
68. J. Mei, N. Zhang, J. Friend, Fabrication of surface acoustic wave devices on lithium niobate. *J. Vis. Exp.* **160**, e61013 (2020).
69. B. G. Chung, A. Manbachi, A. Khademhosseini, A microfluidic device with groove patterns for studying cellular behavior. *J. Vis. Exp.* **7**, **e270**, (2007).
70. J. Gu, Y. Jing, Modeling of wave propagation for medical ultrasound: A review. *IEEE Trans. Ultrason. Ferroelectr. Freq. Control* **62**, 1979–1992 (2015).
71. L. Shen, Z. Tian, J. Zhang, H. Zhu, K. Yang, T. Li, J. Rich, N. Upreti, N. Hao, Z. Pei, G. Jin, S. Yang, Y. Liang, W. Chaohui, T. J. Huang, Acousto-dielectric tweezers for size-insensitive manipulation and biophysical characterization of single cells. *Biosens. Bioelectron.* **224**, 115061 (2023).

Acknowledgments

Funding: We acknowledge the support from the National Science Foundation (CMMI-2104526 and CMMI-2243771), the National Science Foundation Graduate Research Fellowship Program (2139754), and the National Institutes of Health (R01GM144417). **Author contributions:** L.S. conceived the idea; developed the models for simulations; and designed, fabricated, and characterized acousto-dielectric devices. K.Y. and J.Z. fabricated the acousto-dielectric devices. L.S., J.X., N.H., C.C., and Z.P. conducted the experiments. L.S. analyzed the data. L.S., Z.T., J.R., B.L., W.C., and T.J.H. wrote the paper. T.J.H. and Z.T. supervised the study. **Competing interests:** T.J.H. has cofounded a start-up company, Ascent Bio-Nano Technologies Inc., to commercialize technologies involving acoustofluidics and acoustic tweezers. All other authors declare that they have no competing interests. **Data and materials availability:** All data needed to evaluate the conclusions in the paper are present in the paper and/or the Supplementary Materials. Additional data related to this paper may be requested from the authors.

Submitted 26 February 2024
Accepted 1 July 2024
Published 7 August 2024
10.1126/sciadv.ado8992